Steel and Composite Structures, *Vol. 29, No. 2 (2018) 175-186*
DOI: https://doi.org/10.12989/scs.2018.29.2.175

A force-based element for direct analysis using stress-resultant plasticity model

Zuo-Lei Du [a], Yao-Peng Liu [*] and Siu-Lai Chan [b]

Department of Civil and Environmental Engineering, The Hong Kong Polytechnic University, Hong Kong, China

(*Received February 24, 2018, Revised August 2, 2018, Accepted August 28, 2018*)

Abstract. The plastic hinge method and the plastic zone method are extensively adopted in displacement-based elements and force-based elements respectively for second-order inelastic analysis. The former enhances the computational efficiency with relatively less accurate results while the latter precisely predicts the structural behavior but generally requires more computer time. The displacement-based elements receive criticism mainly on plasticity dominated problems not only in accuracy but also in longer computer time to redistribute the forces due to formation of plastic hinges. The multi-element-per-member model relieves this problem to some extent but will induce a new problem in modeling of member initial imperfections required in design codes for direct analysis. On the contrary, a force-based element with several integration points is sufficient for material yielding. However, use of more integration points or elements associated with fiber section reduces computational efficiency. In this paper, a new force-based element equipped with stress-resultant plasticity model with minimal computational cost is proposed for second-order inelastic analysis. This element is able to take the member initial bowing into account such that one-element-per-member model is adequate and complied with the codified requirements of direct analysis. This innovative solution is new and practical for routine design. Finally, several examples demonstrate the validity and accuracy of the proposed method.

Keywords: second-order inelastic analysis; force-based; steel structures; initial imperfection; stress-resultant plasticity model

1. Introduction

Many modern design codes, such as AISC360 (2016), Eurocode 3 (2005) and AS4100 (2000), have specified "Direct analysis", "Second-order Analysis" or "Advanced Analysis" for daily design of steel structures, throught which the structural stability and safety can be assessed by checking the members and the system in an integrated manner rather than checking individual member using the effective length method (ELM). The ELM is simply based on the traditional linear analysis without consideration of many effects while the direct analysis method (DAM) considers the major factors affecting system and member strength, for example, second-order $P-\Delta$ and $P-\delta$ effects, initial geometrical imperfections, residual stress, material yielding and joint finite stiffness.

Several different beam-column elements have been proposed to incorporate initial geometrical imperfection at the element level. Chan and Zhou (1995) and Liu *et al*. (2014, 2016) proposed displacement-based beam-column elements considering initial bowing for second-order direct analysis, which show high computational efficiency and accuracy. Chiorean (2017) and Du *et al*. (2017) proposed two force-based elements into which can also directly incorporate initial imperfection in different manners and exhibit high performance when using one-element-per-member model.

In terms of material nonlinearity, there are two widely used methods, i.e., plastic hinge method and plastic zone method. The former method (also named as concentrated plasticity method) is extensively adopted in the displacement-based beam-column elements due to its simplicity and computational efficiency such as Liew *et al*. (1993a, b) and Farahi and Erfani (2017), while the latter method (also well-known as distributed plasticity method) is usually used to calibrate the accuracy of plastic hinge method in previous research. Although the latter can obtain more accurate results such as the three-dimensional finite element model (Dai and Lam 2014, Yan *et al*. 2017, Ding *et al*. 2017, Keykha 2017), it costs more computer time as well as computer storage in analysis as it is required to mesh a section into a number of fibers and several integration points are needed along the member length (Nguyen and Kim 2016). This problem will be more serious in the nonlinear dynamic (time-history) analysis, especially generating IDA curves (Khaloo *et al*. 2016, Tirca *et al*. 2015, Parghi and Alam 2017). With recently fast development of computer hardware, it is possible to adopt the plastic zone method in the second-order inelastic analysis so that the structural behavior can be well predicted. However, the lack of consideration of initial imperfection in traditional force-based elements and tedious determination of fiber state require too many computer resources, especially for high-rise buildings and long-span

*Corresponding author, Senior Research Fellow,
E-mail: yp.liu@polyu.edu.hk
[a] Ph.D. Student, E-mail: zuolei.du@gmail.com
[b] Chair Professor, E-mail: ceslchan@polyu.edu.hk

ISSN: 1229-9367 (Print), 1598-6233 (Online)

structures. Thus, it is urgent to improve the current analysis method so that more accurate results can be provided for safer design with enhancement of computational efficiency.

Generalized plasticity method was firstly proposed by Auricchio and Taylor (1995) for material yielding and then extended to a stress resultant section model used in the beam-column element developed by Kostic *et al*. (2013). Their element adopts concentrated plasticity model, whose feature is described by the generalized plasticity theory using yield and limit surfaces. Thus, their method can take the benefit of well-accepted interaction functions between the axial force and the bending moments specified in design codes or more accurate yield functions in literature. However, the plastic hinges can only be formed at the ends of the element. It means that more elements are required if one or more plastic hinges are formed along the member. Further, their study does not take the $P-\delta$ effect into account and as a result their outcome cannot fulfill the requirement of direct analysis.

This paper is intended to improve the computational efficiency of the force-based element with distributed plasticity proposed by Du *et al*. (2017). The time-consuming fiber section integration will be replaced by the robust stress-resultant plasticity model based on the concept of the generalized plasticity method. As the discretization of cross-section into fibers is no longer required, the proposed method will significantly reduce the computer time by directly using the relationship between section deformations and stress resultants. The backward-Euler algorithm is used in the determination of section state and good numerical convergence is observed. The proposed method makes the practical application of force-based element in design of engineering structures but not simply as an academic tool. This effort has not been conducted in previous research. More importantly, this solution meets the code requirements for second-order direct analysis. This paper attempts to fill the gap between the research and the practical application so that a better design in terms of safety and saving can be achieved.

2. Element formulations

The shape function of beam-column element based on flexibility method is the equation of stress resultants. The force equilibrium along a member is always guaranteed even undergoing large deflection and significant yielding, and therefore the force-based elements are generally more accurate than the displacement-based elements. The proposed element incorporates $P-\delta$ effect, material nonlinearity and initial geometrical imperfections in the elemental stiffness matrix such that one element per member is generally adequate for second-order inelastic analysis complying with code requirements.

The Hellinger-Reissner (HR) variational principle, which is expressed in Eq. (1) in terms of displacement field $\mathbf{u}$ and stress field $\boldsymbol{\sigma}$, is adopted to derive the proposed force-based element.

$$\Pi_{HR}(\boldsymbol{\sigma},\mathbf{u}) = \int_{\Omega} [\boldsymbol{\varepsilon}(x,y,z)\boldsymbol{\sigma} - \chi(\boldsymbol{\sigma})]d\Omega + \boldsymbol{\Pi}_{ext}(\mathbf{u}) \quad (1)$$

The stationary of the HR potential can be obtained as below by taking the first variation for Eq. (1) with respect to the displacement and the stress resultant and setting it to zero.

$$\delta\boldsymbol{\Pi}_{HR}(\mathbf{S},\mathbf{u}) = \delta_{\boldsymbol{S}}\boldsymbol{\Pi}_{HR} + \delta_{\boldsymbol{u}}\boldsymbol{\Pi}_{HR} = 0 \quad (2)$$

Thus, the weak form of equilibrium and compatibility equations can be deduced in Eqs. (3) and (4) respectively.

$$\delta_{\boldsymbol{u}}\boldsymbol{\Pi}_{HR} = 0 \quad (3)$$

$$\delta_{\boldsymbol{S}}\boldsymbol{\Pi}_{HR} = 0 \quad (4)$$

The equilibrium equations shown in Eq. (3) are further expanded as

$$\delta_{\boldsymbol{u}}\boldsymbol{\Pi}_{HR} = \int_L \mathbf{S}^T \begin{Bmatrix} \delta u' + v'\delta v' + w'\delta w' + v_0'\delta v' + w_0'\delta w' \\ \delta v'' \\ -\delta w'' \\ \delta\psi' \end{Bmatrix} dx - \overline{\boldsymbol{P}}^{\boldsymbol{T}}\delta\mathbf{D} = 0 \quad (5)$$

in which, $u(x)$, $v(x)$, and $w(x)$ are displacement components; $\psi(x)$ is torsional angle; $v_0(x)$ and $w_0(x)$ are initial geometrical imperfection; the superscript $'$ means differential of x. The section forces $S(x)$ in related with end forces $\mathbf{P}$ are expressed as

$$\mathbf{S}(x) = \begin{Bmatrix} N(x) \\ M_z(x) \\ M_y(x) \\ T(x) \end{Bmatrix} = \mathbf{b}(x)\mathbf{P} \quad (6)$$

The compatibility equations given in Eq. (4) can be written as

$$\delta_{\boldsymbol{S}}\boldsymbol{\Pi}_{HR} = \int_L \delta\mathbf{S}^T \left[\begin{Bmatrix} u' + \frac{1}{2}v'^2 + \frac{1}{2}w'^2 + v'v_0' + w'w_0' \\ v'' \\ -w'' \\ \psi' \end{Bmatrix} - \frac{\partial\chi(\mathbf{S})}{\partial\mathbf{S}} \right] dx = 0 \quad (7)$$

Based on the virtual work principle, there exists a relation between the increment of virtual internal forces and virtual end forces as follows.

$$\int_L \delta\mathbf{S}(x)^T\mathbf{d}(x)dx = \delta\mathbf{P}^T\mathbf{D} \quad (8)$$

The relation between the end displacements $\mathbf{D}$ and the section deformations corresponding to the generalized strains $\mathbf{d}$ along the member can be derived as

$$\mathbf{D} = \int_L \mathbf{b}^*(x)^T\,\mathbf{d}(x)dx \quad (9)$$

The element flexibility matrix can be formed by taking derivative of the end nodal displacements **D** in Eq. (9) with regard to end nodal forces **P** as

$$\mathbf{F}_e = \frac{\partial \mathbf{D}}{\partial \mathbf{P}} = \int_L \left(\frac{\partial \mathbf{b}^*(x)^T}{\partial \mathbf{P}} \mathbf{d}(x) + \mathbf{b}^*(x)^T \frac{\partial \mathbf{d}(x)}{\partial \mathbf{P}} \right) dx = \int_L [\mathbf{b}^*(x)^T \mathbf{f}_s(x) [\mathbf{b}(x) + \mathbf{h}(x)] + \mathbf{g}(x)] dx \tag{10}$$

in which $\mathbf{h}(x)$ and $\mathbf{g}(x)$ are expressed as

$$\mathbf{h}(x) = P_1 \begin{bmatrix} \mathbf{0} \\ \boldsymbol{V}(x) \\ -\boldsymbol{W}(x) \\ \mathbf{0} \end{bmatrix} \tag{11}$$

$$\mathbf{g}(x) = \frac{1}{2}\kappa_z \begin{bmatrix} \boldsymbol{V}(x) \\ \mathbf{0} \\ \mathbf{0} \\ \mathbf{0} \\ \mathbf{0} \end{bmatrix} - \frac{1}{2}\kappa_y \begin{bmatrix} \boldsymbol{W}(x) \\ \mathbf{0} \\ \mathbf{0} \\ \mathbf{0} \\ \mathbf{0} \end{bmatrix} \tag{12}$$

with

$$\boldsymbol{V}(x) = \frac{\partial v(x)}{\partial \boldsymbol{P}} \tag{13}$$

$$\boldsymbol{W}(x) = \frac{\partial w(x)}{\partial \boldsymbol{P}} \tag{14}$$

From the mentioned above, the element flexibility matrix can be determined once the displacements $v(x)$ and $w(x)$ as well as initial imperfections $v_0(x)$ and $w_0(x)$ are known.

To incorporate this new force-based element into the conventional displacement-based program like NIDA (2017), the element stiffness matrix $\mathbf{K}_e$ in basic coordinate system can be obtained as

$$\mathbf{K}_e = \mathbf{F}_e^{-1} \tag{15}$$

in which $\mathbf{F}_e$ is the flexibility matrix defined in Eq. (10).

To transform the quantities from basic system to global system, the co-rotational method used in Chan and Zhou (1994) is adopted here. Similar co-rotational approaches were adopted in Ray *et al*. (2015), Rasmussen *et al*. (2016) and Zubydan *et al*. (2018). Thus, the tangent stiffness matrix $\mathbf{K}_T$ of beam-column element can be calculated as below using the co-rotational framework

$$\mathbf{K}_T = \boldsymbol{L}(\boldsymbol{T}^T \mathbf{K}_e \boldsymbol{T} + \boldsymbol{N})\boldsymbol{L}^T \tag{16}$$

where, $\boldsymbol{L}$, $\boldsymbol{T}$ and $\boldsymbol{N}$ are transformation matrix from local to global system, $\boldsymbol{T}$ is transformation matrix from basic to local system, $\boldsymbol{N}$ is a matrix considering the work due to the initial force and the translational displacements. The matrices $\boldsymbol{L}$, $\boldsymbol{T}$ and $\boldsymbol{N}$ are detailed in Chan and Zhou (1994).

3. Distributed plasticity analysis

The fiber section approach is widely adopted in force-based elements for consideration of distributed plasticity along both the section height and the member length. A cross-section will be discretized into a bunch of fibers to monitor section responses as shown in Fig. 1. Each of them is an independent region, which is defined by its centroid coordinates (y_j, z_j) and area (A_j). Their mechanics behaviors are modeled by a nonlinear stress-strain relationship. The stress resultants and tangent stiffness of the cross-section can be computed by integration of these fibers as

$$\mathbf{S}(\xi_i) = \begin{Bmatrix} N(\xi_i) \\ M_z(\xi_i) \\ M_y(\xi_i) \\ T \end{Bmatrix} = \begin{Bmatrix} \sum_{j=1}^{m} (\sigma_j A_j) \\ \sum_{j=1}^{m} (-y_j \sigma_j A_j) \\ \sum_{j=1}^{m} (z_j \sigma_j A_j) \\ GJ\varphi' \end{Bmatrix} \tag{17}$$

$$\mathbf{k}_s(\xi_i) = \begin{bmatrix} \sum_{j=1}^{m} (E_{tj} A_j) & \sum_{j=1}^{m} (-y_j E_{tj} A_j) & \sum_{j=1}^{m} (z_j E_{tj} A_j) & 0 \\ \sum_{j=1}^{m} (-y_j E_{tj} A_j) & \sum_{j=1}^{m} (y_j^2 E_{tj} A_j) & \sum_{j=1}^{m} (-y_j z_j E_{tj} A_j) & 0 \\ \sum_{j=1}^{m} (z_j E_{tj} A_j) & \sum_{j=1}^{m} (-y_j z_j E_{tj} A_j) & \sum_{j=1}^{m} (z_j^2 E_{tj} A_j) & 0 \\ 0 & 0 & 0 & GJ \end{bmatrix} \tag{18}$$

in which, E_{tj} is the material tangent modulus of the fiber j in related to current stress state.

It should be noted that the progressive yielding of cross-section is reflected by collective effects of fibers, which only need to present in the uniaxial stress state. However, the discretization of cross section before the analysis and the integration for stress resultants and tangent stiffness in the fiber section model requires much computer time and storage, especially in the time-history analysis. A natural idea to resolve this problem is to treat the cross-section as a whole without discretization. One successful application of this idea is the plastic hinge method which has been widely used in the displacement-based elements, for example, Liew *et al*. (1993a, b) and Liu *et al*. (2016). However, their

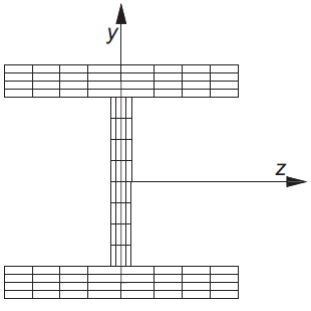

Fig. 1 Fiber discretization for wide-flange section

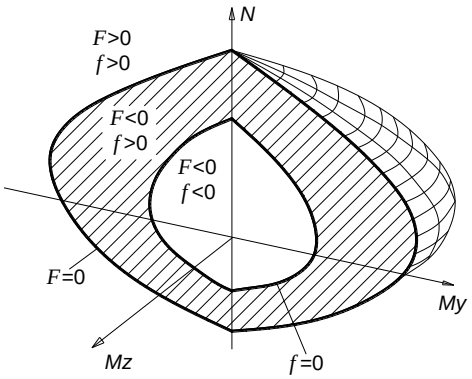

Fig. 2 Yield function and limit function for section state

method needs to increase the load step with small increment so that the progressively yielding behavior can be captured. It will significantly increase computer time. Meanwhile, their method ignores the coupling effect between axial force and bending moments.

In this paper, a stress-resultant plasticity model is proposed to reflect the relationship between the section deformations and the stress resultants directly, which is extended from the generalized plasticity material model introduced by Auricchio and Taylor (1994, 1995) and Lubliner *et al*. (1993). This model is also studied by Kostic *et al*. (2013, 2016) to investigate the inelastic response of plastic hinge. With the yield function f and limit function F as shown in Fig. 2, the stress-resultant plasticity model is able to model the progressive yielding of cross-section. The functions f and F divide the space in terms of P-My-Mz into three regions:

(1) Region 1: $f < 0$ and $F < 0$,
the section is in elastic state;
(2) Region 2: $f > 0$ and $F < 0$,
the section is in inelastic state, or elastic state under unloading;
(3) Region 3: $f > 0$ and $F > 0$,
the section is in inadmissible state.

Unlike the fiber section model which needs numerous variables to record material history state of each fiber during the analysis, the stress-resultant plasticity model only needs a few variables to represent the whole section state. It is clear that this model will save much computer storage and cost less computer time in determination of section state. Further, as the proposed force-based element has taken the initial geometrical imperfections and $P-\delta$ effect into account, only one element per member is able to provide accurate responses for design purpose. This new method will significantly reduce the degrees of freedom and enhance computational efficiency.

4. Stress-resultant plasticity model

To distinguish the section state between elastic and inelastic behaviors, the yield function of the metal material is expressed in terms of stress when using fiber section approach. As an extension of this concept, the fully yield function of a section at the integration point along a member can be expressed in terms of section stress-resultant $\mathbf{p}$ as

$$f(\mathbf{p}) = \Phi(\mathbf{p}-\mathbf{a}) - H_{iso}\,\alpha \tag{19}$$

in which, $\mathbf{a}$ is the center point of the yield surface to consider the Kinematic hardening effect; H_{iso} is the isotropic plastic hardening parameter; α is the equivalent plastic strain.

The gradually yielding process is described by a limit function as given in Eq. (20), which is originally proposed for generalized plasticity model.

$$F = h(f)\frac{d\Phi}{dt} - \dot{\lambda} \tag{20}$$

with

$$\mathrm{h(f)} = \frac{\mathrm{f}}{\delta(\beta - \mathrm{f})} \tag{21}$$

in which, $\dot{\lambda}$ is the plastic strain-rate multiplier; δ and β are two non-dimensional positive constants, and the former controls the speed from elastic state to fully plastic state while the latter represents the region of elastic-plastic state.

When the sectional forces exceed the yield surface, plastic deformation will happen. The plastic deformation is determined by an associated plastic flow rule as

$$\dot{\mathbf{d}}^{p} = \dot{\lambda}\frac{\partial f}{\partial \mathbf{p}} \tag{22}$$

According to the plasticity theory, the Kuhn-Tucker complementarity conditions can be used to convert the plasticity problem to a constrained optimization problem. The complementarity conditions are expressed as

$$\dot{\lambda} \geq 0, \quad F \leq 0 \quad \dot{\lambda}F = 0 \tag{23}$$

Hence, the limit function in Eq. (20) should satisfy the following equation as

$$F = h(f)\frac{d\Phi}{dt} - \dot{\lambda} = 0 \tag{24}$$

5. Integration of rate equations and section tangent stiffness

5.1 Integration algorithm

The section deformations can be decomposed into two parts (i.e., elastic and plastic) as

$$\mathbf{d} = \mathbf{d}^{e} + \mathbf{d}^{p} \tag{25}$$

During the integration process, the section forces and the section deformations are deemed as known at the time step t_n. The relationship between the generalized strain

field and stress resultants is given as

$$\mathbf{s}_n = \mathbf{k}_{se}(\mathbf{d}_n - \mathbf{d}_n^p) \tag{26}$$

where, $\mathbf{k}_{se}$ is the elastic section tangent stiffness matrix; $\mathbf{d}_n$ and $\mathbf{d}_n^p$ are the total section deformations and plastic section deformations respectively; $\mathbf{s}_n$ is the section forces excluding the torsional moment.

If the increment of section deformations is expressed as $\Delta\mathbf{d}$ at time step t_{n+1}, the total section deformations can be determined as

$$\mathbf{d}_{n+1} = \mathbf{d}_n + \Delta\mathbf{d} \tag{27}$$

From the above, the only unknown variable for determination of section state is the plastic section deformations $\mathbf{d}_{n+1}^p$. In this paper, the backward-Euler numerical integration algorithm will be adopted to find the plastic section deformations. This method is based on the following equation

$$\mathbf{d}_{n+1}^p = \mathbf{d}_n^p + \mathbf{r}_{n+1}(\mathbf{s}_{n+1})\Delta\lambda \tag{28}$$

in which

$$\mathbf{r}(\mathbf{s}) = \frac{\partial f}{\partial \mathbf{s}} \tag{29}$$

The incremental form of the Kuhn-Tucker conditions can be represented as

$$\Delta\lambda \geq 0, \quad F_{n+1} \leq 0 \quad \Delta\lambda F = 0 \tag{30}$$

Similarly, the continuous form of the limit function in Eq. (24) can be rewritten to a discrete form as

$$h(f)(\Phi_{n+1} - \Phi_n) - \Delta\lambda = 0 \tag{31}$$

in which

$$\Delta\lambda = \int_{t_n}^{t_{n+1}} \lambda dt \tag{32}$$

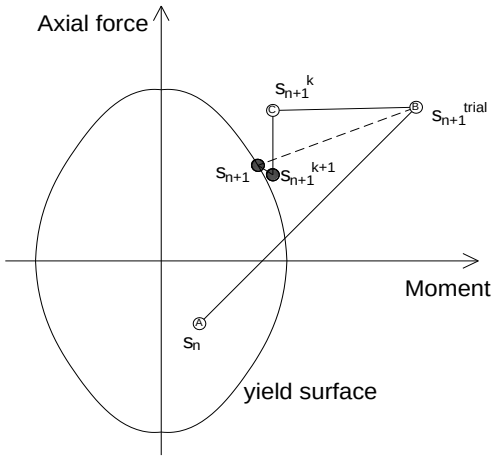

Fig. 3 Backward-Euler return procedure

5.2 Return mapping algorithm

In this paper, the elastic predictor-plastic corrector integration strategy is adopted as the force integration algorithm. When the moment-axial force point lies outside the full yield surface, the procedure of return mapping algorithm as shown in Fig. 3 should be used to correct the section state. The position A is the starting point while the final position can be determined by the following three steps.

Step 1: Prediction procedure

In the first step, the trial position B is located by the elastic relationship between the section deformations and stress resultants given in Eq. (33)

$$\mathbf{s}_{n+1}^{trial} = \mathbf{k}_{se}(\mathbf{d}_{n+1} - \mathbf{d}_n^p) \tag{33}$$

The plastic deformations are assumed to be constant from time step t_n to t_{n+1}. Hence, the plastic deformations at the time step t_{n+1} are equal to that at the time step t_n as shown in Eq. (34), and $\Delta\lambda = 0$.

$$\boldsymbol{d}_{n+1}^{p,trial} = \boldsymbol{d}_n^p \tag{34}$$

Further, the yield function in Eq. (19) will be updated with the trial stress resultants $\mathbf{s}_{n+1}^{trial}$ as

$$f_{n+1}^{trial} = \Phi_{n+1}^{trial} - H_{iso}\alpha \tag{35}$$

Step 2: State check

After trial point B and trial section state are determined from step 1, the trial location should be checked if the conditions in Eq. (30) are satisfied or not. As the plastic flow is frozen at step 1 with $\Delta\lambda = 0$, the conditions can be rewritten as

$$f_{n+1}^{trial} < 0, \quad or \quad f_{n+1}^{trial}(\Phi_{n+1}^{trial} - \Phi_n) \leq 0 \tag{36}$$

The first condition in Eq. (36) represents the state that the stress resultants do not violate the yield surface, and the second one is for the unloading state. If one of the conditions is satisfied, the plastic deformations, stress resultants and the tangent stiffness of the section can be updated by Eqs. (37) to (39) using the trial results from step 1, and then exit the whole return procedure. If the conditions are not satisfied, it should go to step 3 to perform the correction procedure.

$$\boldsymbol{d}_{n+1}^p = \boldsymbol{d}_n^p \tag{37}$$

$$\boldsymbol{s}_{n+1} = \boldsymbol{s}_{n+1}^{trial} \tag{38}$$

$$\mathbf{k}_{n+1} = \mathbf{k}_{se} \tag{39}$$

Step 3: Correction procedure

From step 2, it is known that the trial position B is not the balanced point and further iterative procedure is needed to satisfy the conditions in Eq. (30). The difference between the current deformations and the backward-Euler deforma-

tions is represented by a vector $\mathbf{R}$ which can be determined from Eq. (40) for time step t_{n+1}.

$$\mathbf{R}_{n+1} = -\mathbf{d}_{n+1}^{p} + \mathbf{d}_{n}^{p} + \mathbf{r}_{n+1}\Delta\lambda \tag{40}$$

To find the final deformations meeting the requirements in Eq. (30), all elements in vector $\mathbf{R}$ should be less than a tolerance. For the trial plastic deformations, $\mathbf{d}_{n}^{p}$ being fixed, a truncated Taylor expansion can be applied to Eq. (40) such that a new residual, $\mathbf{R}^{k}$, can be produced as

$$\mathbf{R}^{k} = \mathbf{R}^{0} - \dot{\mathbf{d}}_{n+1}^{p} + \Delta\lambda\mathbf{Q}\dot{\mathbf{s}} + \dot{\lambda}\mathbf{r} \tag{41}$$

with

$$\mathbf{Q}(\mathbf{s}) = \frac{\partial^{2} f}{\partial \mathbf{s}^{2}}, \quad \dot{\mathbf{s}} = -\mathbf{k}_{se}\dot{\mathbf{d}}_{n+1}^{p} \tag{42}$$

in which, $\dot{\mathbf{s}}$ is the change in $\mathbf{s}$; $\dot{\lambda}$ is the change in $\Delta\lambda$. Setting $\mathbf{R}^{k}$ to zero, it gives

$$\dot{\mathbf{d}}_{n+1}^{p} = (\mathbf{I} + \Delta\lambda\mathbf{Q}\mathbf{k}_{se})^{-1}(\mathbf{R}^{0} + \dot{\lambda}\mathbf{r}) \tag{43}$$

With Eq. (43), a truncated Taylor series on Eq. (30) will produce

$$\mathrm{a}\Delta\Delta\lambda + b\Delta\Delta\lambda + c = 0 \tag{44}$$

in which

$$\mathrm{a} = (\delta - \mathbf{r}^{T}\mathbf{C}\mathbf{r})(\mathbf{r}^{T}\mathbf{C}\mathbf{r}) \tag{45}$$

$$\begin{aligned}\mathrm{b} = {} & \delta\Delta\lambda(\mathbf{r}^{T}\mathbf{C}\mathbf{r}) + \delta(\beta - f^{trial} + \mathbf{r}^{T}\mathbf{C}\mathbf{R}_{1}) \\ & + (f^{trial} + \Phi^{trial} - 2\mathbf{r}^{T}\mathbf{C}\mathbf{R}_{1} - \Phi_{n})(\mathbf{r}^{T}\mathbf{C}\mathbf{r})\end{aligned} \tag{46}$$

$$\begin{aligned}\mathrm{c} = {} & \delta\Delta\lambda(\beta - f^{trial} + \mathbf{r}^{T}\mathbf{C}\mathbf{R}_{1}) \\ & -(f^{trial} - \mathbf{r}^{T}\mathbf{C}\mathbf{R}_{1})(\Phi^{trial} - \mathbf{r}^{T}\mathbf{C}\mathbf{R}_{1} - \Phi_{n})\end{aligned} \tag{47}$$

$$\mathbf{C} = (\mathbf{k}_{se}{}^{-1} + \Delta\lambda\mathbf{Q})^{-1} \tag{48}$$

The smaller positive solution $\Delta\Delta\lambda$ in Eq. (44) will be used to update $\Delta\lambda$ on iteration k as

$$\Delta\lambda_{n+1}^{k+1} = \Delta\lambda_{n+1}^{k} + \Delta\Delta\lambda_{n+1}^{k} \tag{49}$$

When $\Delta\Delta\lambda$ is less than the given tolerance, the final force position is located and the whole process is terminated. Otherwise, the iterative procedure using Eq. (49) should be continued until $\Delta\Delta\lambda$ meets the convergent condition.

5.3 Section tangent stiffness matrix

After determination of the section state by the return mapping algorithm above, the section tangent stiffness can be calculated. The standard backward-Euler algorithm in Eq. (28) can be rewritten as

$$\mathbf{s}_{n+1} = \mathbf{s}_{n+1}^{trial} - \Delta\lambda\mathbf{k}_{se}\mathbf{r} \tag{50}$$

Taking derivative of Eq. (50), it gives

$$\dot{\mathbf{s}}_{n+1} = \mathbf{k}_{se}\dot{\mathbf{d}} - \dot{\lambda}\mathbf{k}_{se}\mathbf{r} - \Delta\lambda\mathbf{k}_{se}\dot{\mathbf{s}}_{n+1} \tag{51}$$

To satisfy Eq. (31), the consistent tangent matrix can be derived as

$$\mathbf{k}_{n+1} = \mathbf{C}_{n+1} - k\mathbf{C}_{n+1}\mathbf{r}_{n+1}\mathbf{r}_{n+1}^{T}\mathbf{C}_{n+1} \tag{52}$$

in which

$$k = \frac{(f_{n+1} + \Phi_{n+1} - \Phi_{n} + \delta\Delta\lambda_{n+1})}{\delta(\beta - f_{n+1}) + (f_{n+1} + \Phi_{n+1} - \Phi_{n} + \delta\Delta\lambda_{n+1})\mathbf{r}^{T}\mathbf{C}_{n+1}\mathbf{r}} \tag{53}$$

6. Verification examples

For the steel member with wide-flange compact section, Orbison *et al*. (1982) proposed a well-accepted yield function which is reproduced in Eqs. (54) and (55) below to trace the material nonlinearity in this study

$$\begin{aligned}\Phi(\mathrm{F}) = {} & 1.15p^{2} + m_{z}^{2} + m_{y}^{2} + 3.67p^{2}m_{z}^{2} \\ & + 3p^{6}m_{y}^{2} + 4.65m_{y}^{2}m_{z}^{4} = 1\end{aligned} \tag{54}$$

$$\mathrm{F}(P, M_{z}, M_{y}) = \begin{bmatrix} p \\ m_{z} \\ m_{y} \end{bmatrix} = \begin{bmatrix} \dfrac{P}{P_{y}} \\ \dfrac{M_{z}}{M_{pz}} \\ \dfrac{M_{y}}{M_{py}} \end{bmatrix} \tag{55}$$

in which, P_{y} is the axial resistance, M_{pz} and M_{py} are the plastic moment resistance about z- and y-axis respectively. Biglari *et al*. (2014) and Thai *et al*. (2016) employed this yielding surface to model the degradation of stiffness and strength. For easy comparison, the Kinematic and isotropic hardening effects in Eq. (21) are ignored in the following examples.

For fair comparison in terms of computational efficiency, all examples were analyzed in the same personal computer with an Intel® Core™ i7-3770 CPU of 3.4 GHz and 16 GB RAM.

6.1 A cantilever column subjected to cyclic axial force

The cantilever column as shown in Fig. 4 was firstly studied by Kostic *et al*. (2013) using a beam-column element with end plastic hinges only. Here, this example is used to validate the ability of the proposed element in dealing with both material and geometrical nonlinearities using the stress-resultant plasticity model. To demonstrate the accuracy of the proposed method, the fiber section plasticity model will be used for calibration purpose. The layout, section and material properties of the column are shown in Fig. 4. Two cases have been studied as follows.

Case 1: The column without initial geometrical imperfection is subjected to a uniaxial tip translation history along the weak y-axis.

Case 2: The column, with or without initial geometrical imperfection L/300, is subjected to a variable axial force.

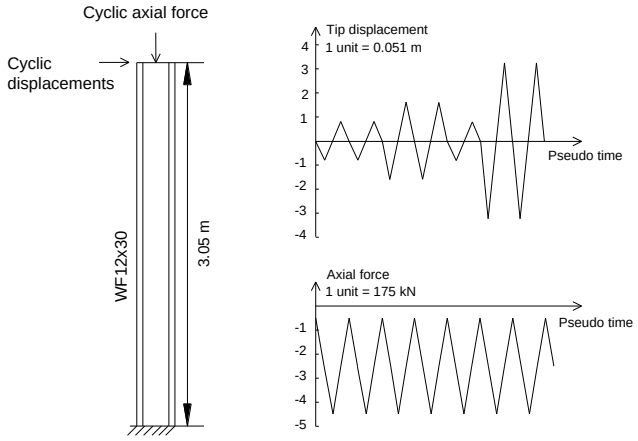

Fig. 4 Layout of cantilever column and loading patterns

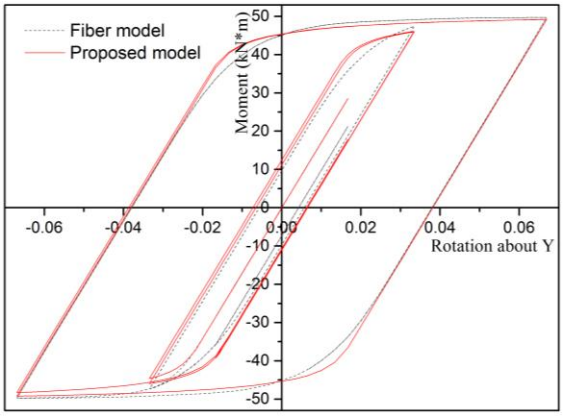

Fig. 5 Bending moment-plastic rotation about y-axis for case 1

In the Case 1, both the proposed stress-resultant plasticity model and the fiber section model are used to simulate the column behavior. Only one force-based element is used in the two methods so that the performance the proposed method can objectively assessed.

The hysteresis curves of bending moment versus rotation on the bottom of column, predicted by two different models, are shown in Fig. 5. It can be seen that the results from the stress-resultant plasticity model are remarkably close to the fiber section model which can be treated as an "exact" solution. It demonstrates that the proposed model is able to capture the gradually yielding of the cross section with acceptable accuracy.

In the Case 2, the column, with and without initial geometrical imperfection, is modelled by one proposed force-based element using the stress-resultant plasticity model. The initial bowing of the column is taken as L/300, which L is the member length. This case aims to study the influence of initial imperfection on the structural behavior.

The hysteresis curves of bending moment versus rotation at the bottom of the column with and without consideration of imperfection are plotted in Fig. 6. It is interesting to find that the initial imperfection has little effect on tension capacity, but it will weaken the column's compressive capacity and alter the structural behavior. It

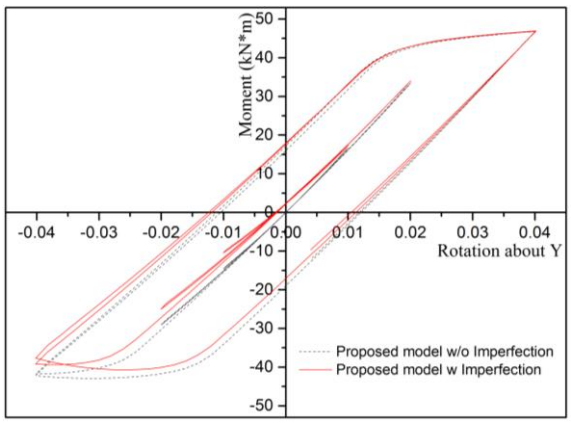

Fig. 6 Bending moment-plastic rotation about y-axis for case 2

also demonstrates that the proposed force-based element with the stress-resultant plasticity model has a good performance under the pseudo static load.

6.2 Vogel six-story steel frame

A two-bay six-story 2D steel frame subjected to distributed gravity loads and concentrated lateral loads at each story level was firstly studied by Vogel (1985), and then studied by Saritas and Koseoglu (2015), Yu and Zhu (2016). The layout, applied loads, section and material properties of the structure are given in Fig. 7. This frame will be used to calibrate accuracy and numerical stability of the proposed method with the stress-resultant plasticity model. The result using several force-based elements per member with fiber section model is believed as a sufficiently accurate response for calibration purpose. The influence of initial out-of-plumb straightness is neglected for easy comparison. Two simulation strategies are designed as follows:

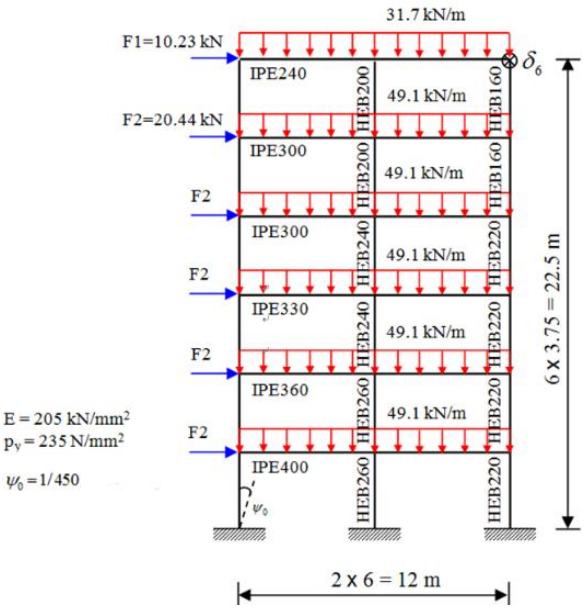

Fig. 7 Layout and loading pattern of the Vogel's six-story frame

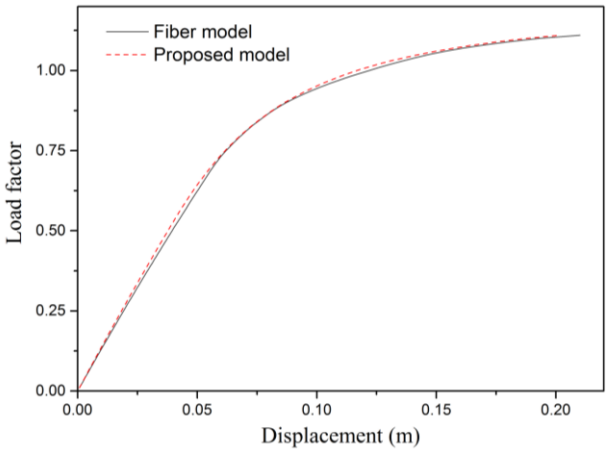

Fig. 8 Horizontal displacement of the Vogel's six-story frame

Case 1: All beams and columns are modelled by one force-based element with the stress-resultant plasticity model. Seven Gauss-Lobatto integration points along each element are employed.

Case 2: All beams are modelled by four proposed elements while all columns are modelled by two force-based elements. The fiber section model is adopted for consideration of material nonlinearity. Seven Gauss-Lobatto integration points along each element are employed.

The load-deflection curve of the node A at the top level is plotted in Fig. 8. It can be seen that the proposed method produces very accurate results, compared with the fiber section approach which consumes more computer time. Thus, this example demonstrates that the proposed method is able to accurately predict the responses of practical structures with one-element-per-member model.

6.3 Two-story high strength steel frame

Six full-scale tests of single-bay two-story frames under cyclic loading were conducted by Hu *et al*. (2017) to study

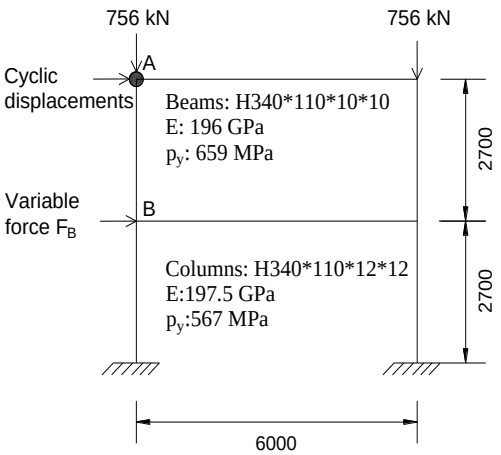

Fig. 9 Layout and loading pattern of the high strength steel frame (Unit: mm)

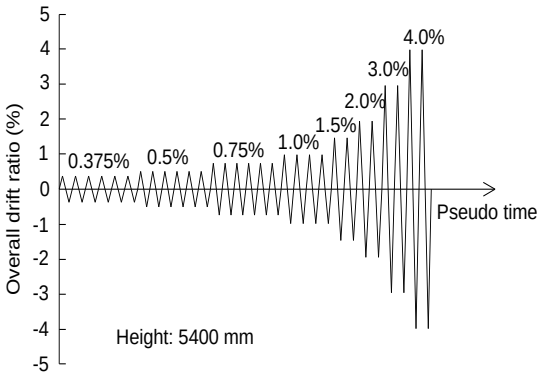

Fig. 10 Loading protocol for the top displacement

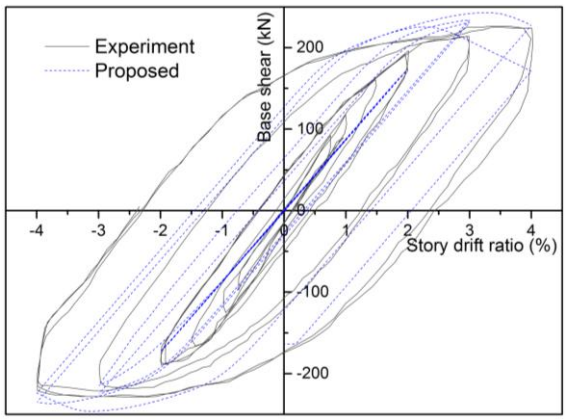

Fig. 11 Base shear versus overall drift ratio

the seismic behavior of high strength steel frames. In this study, the specimen B460-C460-2 with clear presentation of results in their paper for easy comparison is selected to verify the proposed element with the stress-resultant plasticity model. The layout, section and material properties of the specimen are shown in Fig. 9.

A constant axial load of 756 kN is applied on the top of each column. The point A is subjected to a lateral cyclic displacement as shown in Fig. 10. At the same time, a variable force F_B is applied on point B. The force F_B is taken as one twentieth of the lateral reaction force of point A, which is resistant force determined in the last cycle. All beams and columns are modeled by one force-based element. The yielding behavior of the frame is captured by the stress-resultant plasticity model.

The hysteresis results of the base shear versus controlled overall drift ratio against the experimental results is plotted in Fig. 11. Generally speaking, the proposed method can predict the energy absorbing ability through the inelastic behavior of steel members. The numerical simulation results by the proposed method are slightly higher than the experimental results. It may be due to ignorance of the contribution of connections on the absorption of energy in numerical simulation.

6.4 Four-story 3D steel frame

The four-story 3D streel frame with irregular layout

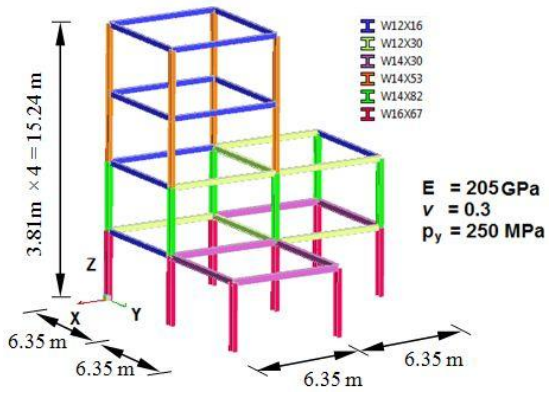

Fig. 12 Layout of four-story 3D steel frame

both in plan and elevation under different ground motions as shown in Fig. 12 is used to study the computational efficiency of the proposed method against the conventional fiber section approach. The structural geometry, section sizes and material properties are detailed in Fig. 12. For simplicity, the static loads on the frame consist of self-weight (SW), 5 kPa of dead loads (DL) and 2 kPa of live loads (LL) applied at each floor before seismic actions. The algorithm for consideration of load sequences can be referred to Liu and Chan (2011). The combination of static loads is 1.0(SW+DL) + 0.5LL, which is also used as the input of mass sources. For the ground motions, four earthquake records are studied here, i.e., El-Centro 1940, San Fernando 1971, Loma Prieta 1989 and Northridge 1994.

All beams and columns are modeled by one proposed element. The material nonlinearity is considered by the stress-resultant plasticity model and fiber section model respectively so that the advantage of proposed method can be quantified based on their cost on computer time. The Newmark method with $\gamma = 0.5$ and $\beta = 0.25$ is adopted for time integration. The Rayleigh damping is calculated by the first two frequencies of the elastic structure. The time increment is 0.02 second.

The base shear F_x and displacement U_x at the roof level are shown in Figs. 13 and 14. It can be seen that both the base shears and the roof displacements from the proposed method are well agreed with the fiber section model.

The times consumed using two different methods in related to four ground motions is shown in Fig. 15. It is observed that the total computer times obtained from the proposed method are shorter than the fiber approach and the minimum time saving is above 25%. Thus, the proposed method can provide sufficiently accurate results with significant reduction on computational cost. This method is ready for design of practical structures.

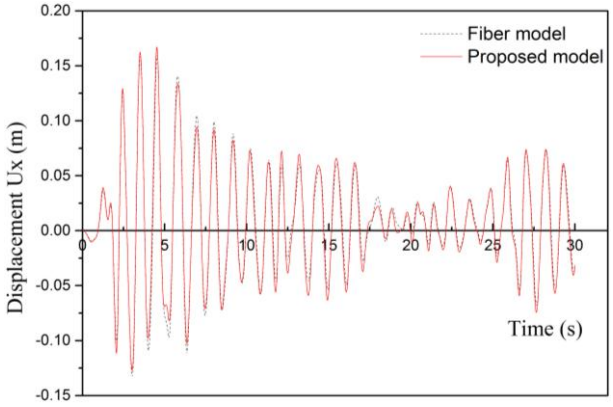

(a) El Centro 1940

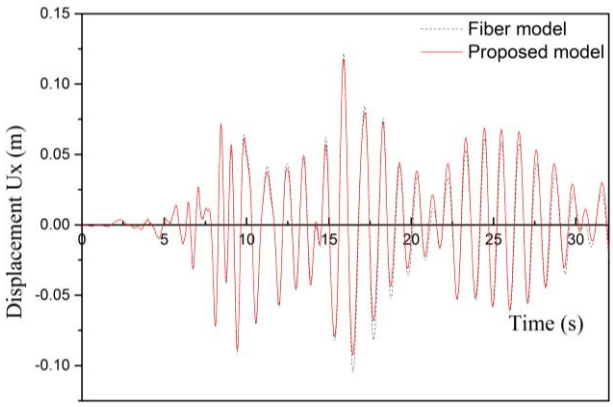

(b) Loma Prieta 1989

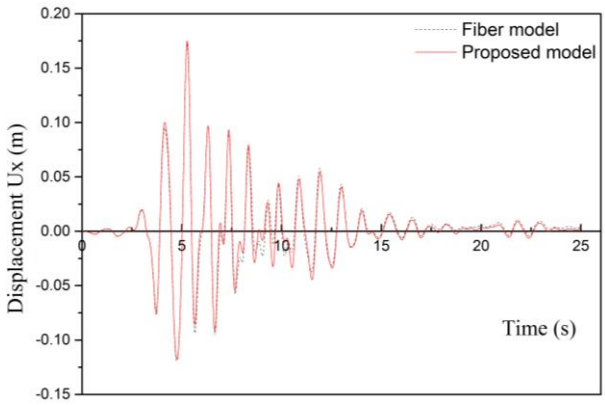

(c) Northridge 1994

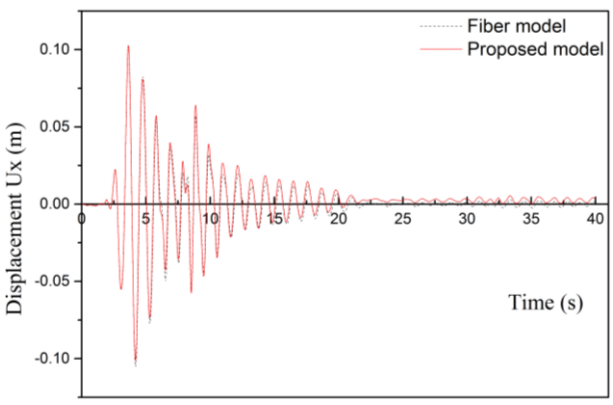

(d) San Fernando 1971

Fig. 13 Displacement under four earthquakes

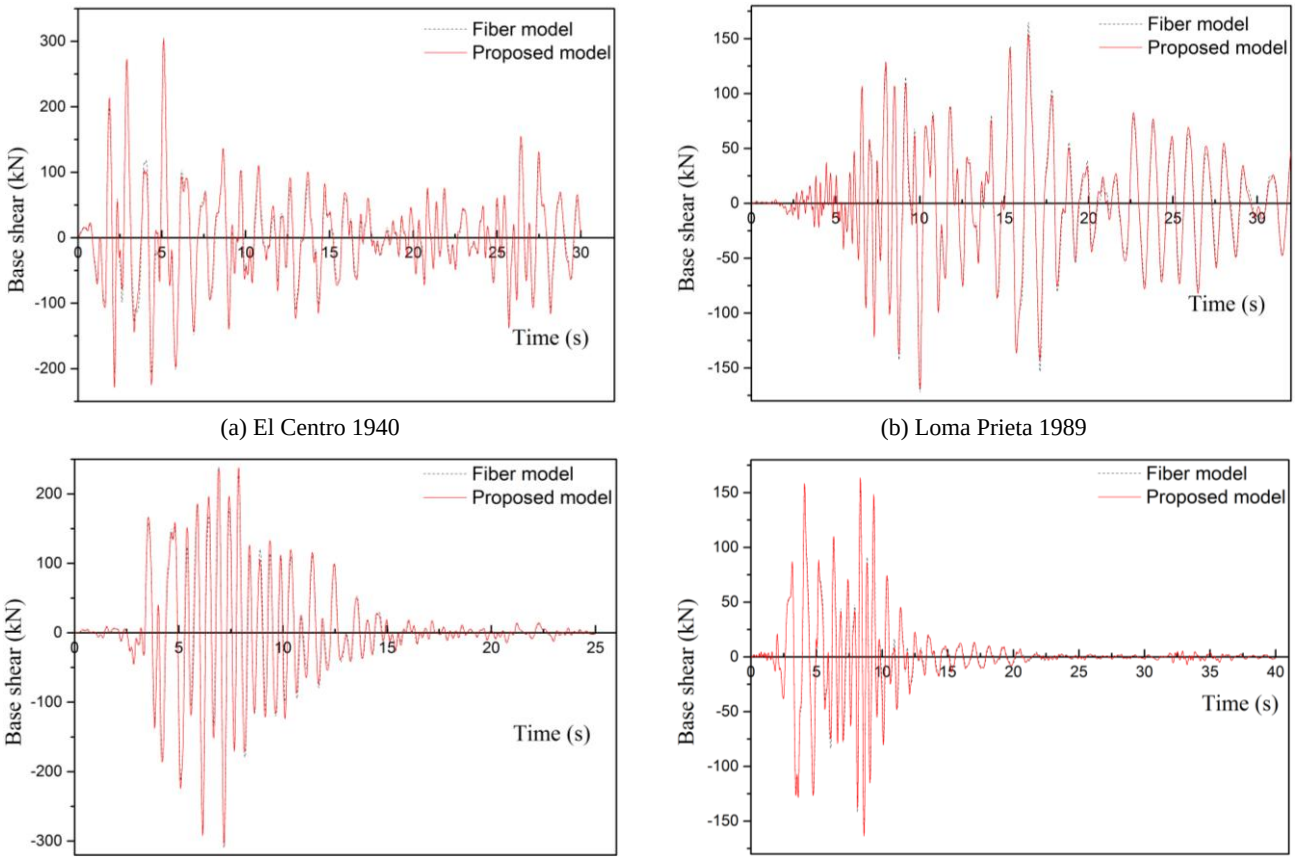

(a) El Centro 1940 (b) Loma Prieta 1989

(c) Northridge 1994 (d) San Fernando 1971

Fig. 14 Base shear under four earthquakes

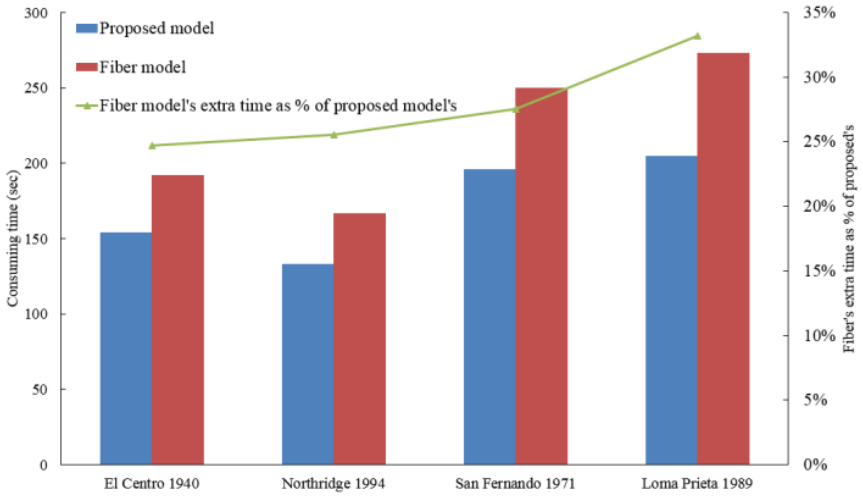

Fig. 15 Computer time under four earthquakes

7. Conclusions

The conventional force-based beam-column elements show high accuracy in inelastic analysis, but they are rarely adopted in global analysis of engineering structures owing to huge consumption of computer time and storage. Also, the conventional method did not take the member initial imperfection into account and as a result they require several elements per member to capture the real behavior and fulfill the requirement of direct analysis.

This paper fills the gap between the research and the practical application as a result the better design in terms of safety and saving can be achieved. The stress-resultant plasticity model is introduced into a robust force-based element developed by the authors to replace the commonly used fiber section model which generally consumes much computer time. Several integration points along an element are used to trace the distributed plasticity. The backward-

Euler algorithm is adopted to determine complex section state which may undergo loading, unloading and re-loading behavior. This algorithm is reliable with good numerical convergence rate.

The numerical examples show that the proposed method can not only predict accurate results as obtained from the conventional fiber section model, but also significantly reduce the computational cost. Thus, this innovative solution, which is complied with the codified requirement of second-order direct analysis, is ready for routine design of practical structures.

Acknowledgments

The authors are grateful for financial support from the Research Grant Council of the Hong Kong SAR Government on the projects "Second-order Analysis of Shallow Dome Structures made of Tapering Members (PolyU 152047/17E)" and "Second-Order Analysis of Flexible Steel Cable Nets Supporting Debris (PolyU 152008/15E) "; from the Innovation and Technology Fund of the Hong Kong SAR Government for the project "Development of an Energy Absorbing Device for Flexible Rock-Fall Barriers (ITS/059/16FP) "; and from the Hong Kong Branch of the Chinese National Engineering Research Centre for Steel Construction of The Innovation and Technology Fund of the Hong Kong SAR Government for the project "Advanced Numerical Analyses for Building Structures Using High Performance Steel Materials".

References

AISC360 (2016), Specification for Structural Steel Buildings; *AISC, Inc., One East Wacker Driver, Suite 700*, Chicago, IL, USA, 60601-1802.

AS4100 (2000), AS4100-1998: Steel Structures; Standard Australia, Sydney.

Auricchio, F. and Taylor, R.L. (1994), "A generalized elastoplastic plate theory and its algorithmic implementation", *International J. Numer. Method. Eng.*, **37**(15), 2583-2608.

Auricchio, F. and Taylor, R.L. (1995), "Two material models for cyclic plasticity: nonlinear kinematic hardening and generalized plasticity", *Int. J. Plastic.*, **11**(1), 65-98.

Biglari, A., Harrison, P. and Bićanić, N. (2014), "Quasi-hinge beam element implemented within the hybrid force-based method", *Comput. Struct.*, **137**, 31-46.

Chan, S.L. and Zhou, Z.H. (1994), "Pointwise equilibrating polynomial element for nonlinear analysis of frames", *J. Struct. Eng.*, **120**(6), 1703-1717.

Chan, S.L. and Zhou, Z.H. (1995), "Second-order elastic analysis of frames using single imperfect element per member", *J. Struct. Eng.-ASCE*, **121**(6), 939-945.

Chiorean, C.G. (2017), "Second-order flexibility-based model for nonlinear inelastic analysis of 3D semi-rigid steel frameworks", *Eng. Struct.*, **136**, 547-579.

Dai, X. and Lam, D. (2014), "A numerical study on the effect of concrete infill and intumescent coating to fire-resistant behaviour of stub elliptical steel hollow sections under axial compression", *Adv. Steel Constr.*, **10**(3), 310-324.

Ding, F.X., Ding, X.Z., Liu, X.M., Wang, H.B., Yu, Z.W. and Fang, C.J. (2017), "Mechanical behavior of elliptical concrete-filled steel tubular stub columns under axial loading", *Steel Compos. Struct., Int. J.*, **25**(3), 375-388.

Du, Z.L., Liu, Y.P. and Chan, S.L. (2017), "A second-order flexibility-based beam-column element with member imperfection", *Eng. Struct.*, **143**, 410-426.

Eurocode 3 (2005), EN 1993-1-1: Design of steel structures - General rules and rules for buildings; European Committee for Standardization.

Farahi, M. and Erfani, S. (2017), "Employing a fiber-based finite-length plastic hinge model for representing the cyclic and seismic behaviour of hollow steel columns", *Steel Compos. Struct., Int. J.*, **23**(5), 501-516.

Hu, F., Shi, G. and Shi, Y. (2017), "Experimental study on seismic behavior of high strength steel frames: Global response", *Eng. Struct.*, **131**, 163-179.

Keykha, A.H. (2017), "CFRP strengthening of steel columns subjected to eccentric compression loading", *Steel Compos. Struct., Int. J.*, **23**(1), 87-94.

Khaloo, A., Nozhati, S., Masoomi, H. and Faghihmaleki, H. (2016), "Influence of earthquake record truncation on fragility curves of RC frames with different damage indices", *J. Build. Eng.*, **7**, 23-30.

Kostic, S.M., Filippou, F.C. and Lee, C.-L. (2013), "In efficient beam-column element for inelastic 3D frame analysis" In: *Computational Methods in Earthquake Engineering*, Springer, pp. 49-67.

Kostic, S.M., Filippou, F.C. and Deretic-Stojanovic, B. (2016), "Generalized plasticity model for inelastic RCFT column response", *Comput. Struct.*, **168**, 56-67.

Liew, J.R., White, D.W. and Chen, W.F. (1993a), "Second-order refined plastic-hinge analysis for frame design. Part I", *Journal of Structural Engineering*, **119**(11), 3196-3216.

Liew, J.R., White, D.W. and Chen, W.F. (1993b), "Second-order refined plastic-hinge analysis for frame design. Part II", *J. Struct. Eng.*, **119**(11), 3217-3236.

Liu, Y.P. and Chan, S.L. (2011), "Second-Order and Advanced Analysis of Structures Allowing for Load and Construction Sequences", *Adv. Struct. Eng.*, **14**(4), 635-646.

Liu, S.W., Liu, Y.P. and Chan, S.L. (2014), "Direct analysis by an arbitrarily-located-plastic-hinge element - Part 1: Planar analysis", *J. Constr. Steel Res.*, **103**, 303-315.

Liu, S.W., Bai, R., Chan, S.L. and Liu, Y.P. (2016), "Second-order direct analysis of domelike structures consisting of tapered members with I-sections", *J. Struct. Eng.*, **142**(5), 04016009.

Lubliner, J., Taylor, R.L. and Auricchio, F. (1993), "A new model of generalized plasticity and its numerical implementation", *Int. J. Solids Struct.*, **30**(22), 3171-3184.

NIDA (2017), User's Manual, Nonlinear Integrated Design and Analysis; NIDA 9.0 HTML Online Documentation. http://www.nidacse.com/manuals/nida9.pdf

Nguyen, P.C. and Kim, S.E. (2016), "Advanced analysis for planar steel frames with semi-rigid connections using plastic-zone method", *Steel Compos. Struct., Int. J.*, **21**(5), 1121-1144.

Orbison, J.G., McGuire, W. and Abel, J.F. (1982), "Yield surface applications in nonlinear steel frame analysis", *Comput. Method. Appl. Mech. Eng.*, **33**(1-3), 557-573.

Parghi, A. and Alam, M.S. (2017), "Seismic collapse assessment of non-seismically designed circular RC bridge piers retrofitted with FRP composites", *Compos. Struct.*, **160**, 901-916.

Rasmussen, K.J., Zhang, X. and Zhang, H. (2016), "Beam-element-based analysis of locally and/or distortionally buckled members: Theory", *Thin-Wall. Struct.*, **98**, 285-292.

Ray, T., Schachter-Adaros, M. and Reinhorn, A.M. (2015), "Flexibility-Corotational Formulation of Space Frames with Large Elastic Deformations and Buckling", *Comput.-Aided Civil Infrastruct. Eng.*, **30**(1), 54-67.

Saritas, A. and Koseoglu, A. (2015), "Distributed inelasticity planar frame element with localized semi-rigid connections for

nonlinear analysis of steel structures", *Int. J. Mech. Sci*., **96**, 216-231.
Thai, H.T., Uy, B., Kang, W.H. and Hicks, S. (2016), "System reliability evaluation of steel frames with semi-rigid connections", *J. Constr. Steel Res*., **121**, 29-39.
Tirca, L., Chen, L. and Tremblay, R. (2015), "Assessing collapse safety of CBF buildings subjected to crustal and subduction earthquakes", *J. Constr. Steel Res*., **115**, 47-61.
Vogel, U. (1985), "Calibrating Frames", *Stahlbau*, **54**, 295-311.
Yan, B., Liu, J. and Zhou, X. (2017), "Axial load behavior and stability strength of circular tubed steel reinforced concrete (SRC) columns", *Steel Compos. Struct., Int. J*., **25**(5), 545-556.
Yu, Y. and Zhu, X. (2016), "Nonlinear dynamic collapse analysis of semi-rigid steel frames based on the finite particle method", *Eng. Struct*., **118**, 383-393.
Zubydan, A.H., ElSabbagh, A.I., Sharaf, T. and Farag, A.E. (2018), "Inelastic large deflection analysis of space steel frames using an equivalent accumulated element", *Eng. Struct*., **162**, 121-134.

DL